Journal of Catalysis 257 (2008) 334–344

Contents lists available at ScienceDirect

Journal of Catalysis

www.elsevier.com/locate/jcat

Reactivity of lanthanum substituted cobaltites toward carbon particles

J.L. Hueso [a,b,*], A. Caballero [a,b], M. Ocaña [a], A.R. González-Elipe [a]

[a] Instituto de Ciencia de Materiales de Sevilla (Centro Mixto CSIC-Universidad de Sevilla), Avda. Américo Vespucio, 49, 41092 Sevilla, Spain
[b] Departamento de Química Inorgánica, Universidad de Sevilla, C/Profesor González 1, 41070 Sevilla, Spain

ARTICLE INFO

Article history:
Received 27 December 2007
Revised 8 May 2008
Accepted 13 May 2008
Available online 16 June 2008

Keywords:
Perovskites
Carbon
XPS
EELS
Temperature-programmed oxidation

ABSTRACT

This work reports on the reactivity toward carbon of a $La_{0.5}Sr_{0.5}CoO_{3-\delta}$ perovskite prepared by spray pyrolysis. It is shown that this perovskite presents a moderate activity for the thermal oxidation of carbon, producing a decrease in its temperature of combustion of ca. 150 °C and a significant increase in the selectivity toward CO_2. Different experiments were carried out with electron energy loss spectroscopy (EELS) and X-ray photoemission spectroscopy (XPS) for the perovskite and its physical mixture with a high-surface area carbon material. In the physical mixture, the cobalt at the surface was partially reduced to Co^{2+} even at room temperature. XPS demonstrated a species of oxygen with low electron density at the catalyst surface. This species seemed to play a significant role in the oxidation processes at the perovskite surface. A model is proposed to account for the changes exhibited by the catalyst during its reaction with carbon.

1. Introduction

Controlling the emission of soot particles from mobile sources, such as diesel engines, represents a major challenge for environmental protection [1,2]. Efficient solutions based on catalysts face the problem that increased efficiency of soot removal is often accompanied by a decrease in the efficiency of NO_x removal [3]. Consequently, most current procedures aim for preferential catalytic removal of NO_x, with soot particles removed with a mixed technology using ceramic filters and oxidation catalysts [4,5]. Among the compounds widely used as active additives for this process are transition metal oxides, like TiO_2, ZrO_2, V_2O_5, CuO, MoO, and CoO [6–13]; rare earth oxides, like La_2O_3 and CeO_2; and mixed systems combining transition metal oxides and alkaline, alkaline-earth, or rare earth elements [13–17]. This latter group also may include perovskites of type ABO_3, where A is a rare-earth element and B is a transition metal. The crystalline structure and the partial substitution of some of their cations by other elements with different oxidation states give these compounds very interesting properties and enhanced activity for the oxidation of soot particles [2,3,5,8,18–20].

Recently, we demonstrated that perovskite catalysts are very efficient for the oxidation of CO in a plasma-catalyst device and that under such conditions, the soot particles even can be beneficial for simultaneous removal of NO and total conversion of CH_4 to CO_2 [21]. In that experiment, carbon was considered to act as a reductive agent toward NO, so that both pollutants were removed simultaneously. But the role of the perovskites in this and other oxidation processes involving soot particles is not completely understood yet. Previous studies have shown that the activity of perovskites as oxidation catalysts may be associated with high mobility of the $O^{=}$ ions of the lattice of this oxide. These ions migrate toward the surface and may provide additional active sites for the oxidation of carbon [4,19,22]. The direct involvement of the oxide ions of the perovskites in the reaction has been further supported by previous studies using isotopic oxygen [23]. In these studies, the finding of two oxygen isotopes in the reaction products clearly shows that the perovskite can provide an additional source of oxygen during oxidation reactions [4,22,23].

Further investigation into the role of the cations in the oxygen-exchange processes, the influence of temperature, and the eventual existence of gradients in stoichiometry between surface and bulk is needed. In an attempt to contribute to this area of study, in the present work we explored the direct interaction of a $La_{0.5}Sr_{0.5}CoO_{3-\delta}$ catalyst (where δ represents the oxygen deficiency of the perovskite) with carbon at either room temperature or increasing temperatures under different conditions. For the purpose of comparison, we also carried out some experiments with a nonsubstituted $LaCoO_3$ perovskite, which have a moderate oxidation reactivity compared with other catalysts [3,8,10,12–14,24,25]. Our use of this perovskite is justified because it allows the possibility of controlling the reactivity toward carbon in such a way that it can be monitored with conventional spectroscopic techniques.

The aim of the present study was to gain insight into the mechanism of interaction of the perovskite with soot and also

* Corresponding author.
E-mail address: jhueso@icmse.csic.es (J.L. Hueso).

0021-9517/$ – see front matter
doi:10.1016/j.jcat.2008.05.012

into how the former may undergo different redox and other chemical processes during real catalytic processes. The perovskites and their mixtures with finely divided carbon were subjected to temperature-programmed oxidation (TPO) analysis and examined by different bulk- and surface-sensitive techniques, including X-ray diffractometry (XRD), electron energy loss spectroscopy (EELS), and X-ray photoemission spectroscopy (XPS). In this latter case, the mixture also was analyzed after in situ heating at increasing temperatures under different atmospheres. To account for the differing results that we obtained, we propose a model that attempts to shed some light on the oxidative catalytic activity of the perovskites and the changes that they undergo when they react with soot particles even after physical grinding at room temperature.

2. Experimental

2.1. Preparation method

The perovskite catalysts used for the present investigation, $La_{0.5}Sr_{0.5}CoO_{3-\delta}$ and $LaCoO_3$, were synthesized by spray pyrolysis [21,26]. The preparation method involved the uniform nebulization of nitrate solutions containing $La(NO_3)_3{\cdot}6H_2O$ (99.99%, Aldrich), $Co(NO_3)_2{\cdot}6H_2O$ (>98%, Fluka), and $Sr(NO_3)_2$ (>99%, Fluka) prepared as a 0.1 M liquid solution of precursors. Two online furnaces, at 250 and 600 °C, evaporated the solvent (distilled water) with the dissolved nitrates and produced an initially amorphous perovskite powder. The material was collected by a porous quartz frit located at the outlet of the heating system. Then the amorphous powders were annealed at 700 °C for 4 h, thus obtaining a crystalline perovskite with rhombohedral symmetry [21,27]. The final catalysts, $LaCoO_3$ and $La_{0.5}Sr_{0.5}CoO_{3-\delta}$, had surface areas of 11 and 13.4 $m^2\,g^{-1}$, respectively.

2.2. Characterization techniques

XRD analysis of the samples before and after treatment was performed in a Siemens D-500 diffractometer working in a Bragg-Bentano configuration and using a Cu anode under an applied voltage of 36 kV and current of 26 mA. XRD spectra were recorded with a step size of 0.02 degrees and an accumulation time of 10 s per step. The SEM images were registered in a field emission scanning electron microscope (FE-SEM) (model S-5200), with an acceleration voltage of 5 kV and current of 10.5 μA. Additional backscattered images also were registered to differentiate light elements (i.e., carbon) and heavy elements (i.e., perovskites) and characterize the distribution of carbon particles after grinding or thermal oxidation. For most experiments (especially the spectroscopic characterization by EELS and XPS), the perovskites were thoroughly ground with a carbon material in a ratio of 9:1 by weight [4] using an agate mortar. The carbon was provided by Cabot and was formed by nanoparticles with a specific surface area of 190 $m^2\,g^{-1}$.

EELS was performed with a Gatan 766-2K spectrometer coupled to a Philips CM 200 transmission electron microscope operating at 200 kV. Background subtraction was done using a standard power law function. A Fourier ratio method [28] was used to eliminate any interference from plasmon contributions. The following edge spectra were recorded using this technique: carbon K, cobalt $L_{2,3}$, and lanthanum $M_{4,5}$. A spectrometer aperture of 2 mm was used for recording the spectra. Under these conditions, a spectral resolution of 1.2 eV was achieved. The Gatan EL/P 3.1 program was used to analyze the spectra. The energy scale of the spectra was calibrated using the lanthanum $M_{4,5}$ edge as an internal standard. The oxidation state of cobalt was assessed using different reference samples containing Co(II), Co(II, III) (CoO and Co_3O_4 from Aldrich), and Co(III) (CoOOH) oxidation states. The CoOOH was prepared by a coprecipitation method described previously [29,30]. The reference samples where mixed with La_2O_3 to simultaneously record the $M_{4,5}$ edge of La that also was used for calibrating the energy scale (i.e., at 831.8 eV) [31]. It is worth noting that under our experimental conditions, EELS analysis can be considered a bulk-sensitive technique.

The XPS spectra were recorded with a Leybold–Heraeous spectrometer working in the pass energy-constant mode at 50 eV and using MgK_α radiation as excitation source. The energy scale of the spectra was calibrated by referencing it to the Sr 3d peak at 133.4 eV [32,33] and to the C 1s peak of the carbon contaminating the surface of the samples at a value of 284.5 eV for the nonsubstituted cobaltite. Both methods yielded similar calibration results. Quantification of the surface concentration of the elements was done by measuring the area under the different peaks after background subtraction according to Shirley's method [34] and applying the sensitivity factors of each element supplied with the spectrometer. To estimate the partition of Co^{3+} and Co^{2+} oxidation states after the different experiments, the recorded Co $2p_{3/2}$ signal was reproduced as a lineal subtraction of the signal due to Co^{2+} recorded from a reference CoO compound [35–37]. The samples were analyzed as introduced in the equipment or after being subjected to different treatments in situ in a preparation chamber connected to the spectrometer. These treatments involved heating in vacuum or under 0.5 Torr O_2 at 400 °C for 30 min.

2.3. Carbon oxidation experiments

Temperature-programmed oxidation (TPO) of carbon in the presence of the perovskites was carried out in a experimental setup described previously [38], consisting of a tubular quartz reactor of 1/8-inch o.d. Temperature was controlled with a thermocouple while the furnace was programmed with lineal ramping of 5 °C min^{-1} up to a maximum temperature of 700 °C. The mixture of gases was adjusted using several mass flow controllers (Bronckhorst). Products were identified with a thermal conductivity detector (TCD) and a quadrupole mass spectrometer (QMS-422 from Baltzers) connected in series with the TPO system. A quantitative calibration of the peak intensities detected in the QMS was previously done with He and the corresponding reactant (O_2) and products (CO and CO_2) expected. The accuracy of the analysis is considered to be within a 10% maximum error [39]. Temperature-programmed desorption (TPD) of the perovskites in the absence of carbon [40] confirmed the mobility of oxygen species from the perovskite and differentiated the possible contribution of carbonates on the CO/CO_2 outlets.

One critical factor influencing the oxidation rate of carbon involves the degree of contact between the catalyst and the carbon particle [10,41,42]. Although ideally, loose contact experiments are preferred, because they more closely mimic the actual working conditions of diesel filters [3,43], we used a tight contact method in this work. No significant variations in temperature conversion and selectivity were observed with respect to the loose contact method under our experimental conditions. The perovskites were ground with 10 wt% of carbon using an agate mortar, and both solids were intimately mixed for 10–15 min. The resulting mixture of 25 mg of total weight was then placed in a quartz wool bed. The reaction mixture was He/O_2 (5%) at a total flow of 25 sccm. An additional experiment in the absence of carbon (including the grinding process) was carried out under identical conditions [40].

3. Results

3.1. Morphological and structural characterization of the perovskites

SEM and XRD analysis provided detailed information on the crystallographic structure and the morphology and particle size of

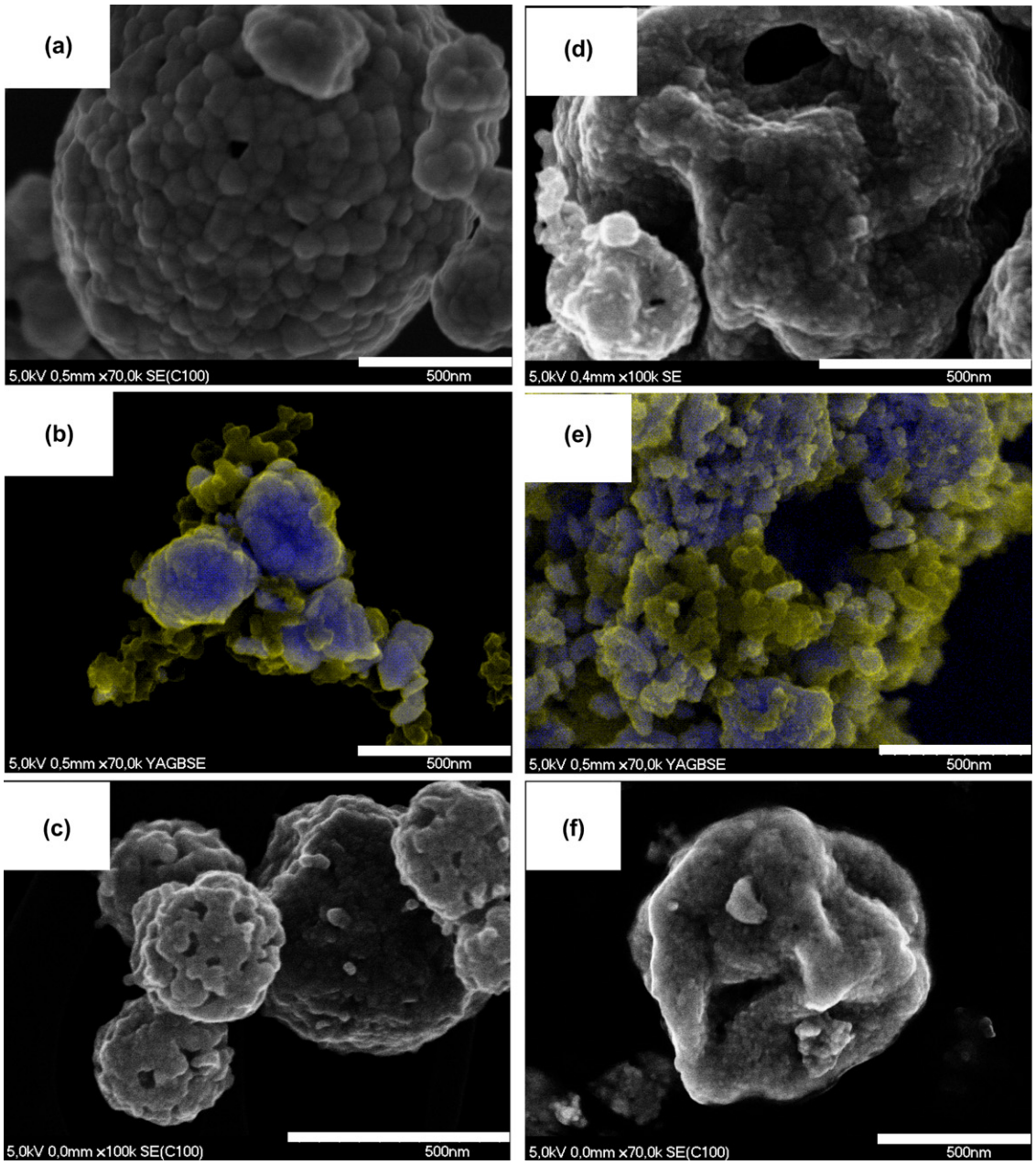

Fig. 1. (Color online). SEM micrographs corresponding to the non-substituted $LaCoO_3$ (left column) and the substituted $La_{0.5}Sr_{0.5}CoO_{3-\delta}$ perovskite (right column) under different experimental situations: (a) and (d) corresponds to the original samples after calcinations at 700 °C; (b) and (e) represents the back-scattered images of the perovskites after grinding with carbon particles at room temperature (blue color for perovskite and yellow for carbon particles); (c) and (f) are referred to the perovskites after the TPO experiments.

the perovskites prepared by spray pyrolysis. The ultrasonic nebulization method of liquid droplets favored the formation of pseudo-spherical particles with a wide range of sizes, as inferred from the SEM analysis results shown in Fig. 1. The mean diameter of particles varied from 200–500 nm to 1 μm, whereas the crystalline domains were much smaller, on the order of 50–90 nm as calculated by applying Scherrer's equation [44] to the main diffraction peaks of the samples (see Table 1 and Fig. 2).

XRD diffractograms revealed a rhombohedral symmetry [21,27] for the $LaCoO_3$ and $La_{0.5}Sr_{0.5}CoO_{3-\delta}$ perovskites. This symmetry limits the use of alternative methods of calculating crystal domain sizes, such as the Williamson–Hall (WH) plots proposed for mixed oxides [43,45–48], because only two well-resolved planes (shown in Fig. 2) may be used in the plot. Fig. 2 shows that this perovskite structure was maintained even after the samples were subjected to different heating and annealing treatments. The XRD patterns also demonstrate that no additional segregated oxides were formed after spray pyrolysis or after the grinding and thermal oxidation treatments (Fig. 2). Only some traces of LaOOH could be detected in the original sample of the nonsubstituted perovskite (Figs. 2a and 2b (left)), likely due to the reaction of lanthanum with ambient conditions [10] and the appearance of some $SrCO_3$ after the thermal oxidation treatment of the doped perovskite (Fig. 2c (right)). In addition, analysis of the backscattered SEM images, in which the carbon particles can be discerned from the heavier perovskite atoms, also revealed that (i) the grinding process favored intimate contact between the carbon particles and the perovskites (Fig. 2b and 2e) in the grinding process and (ii) no appreciable rests of carbonaceous particles could be seen after the thermal oxidation process. Table 1 shows the width of the (024) diffraction

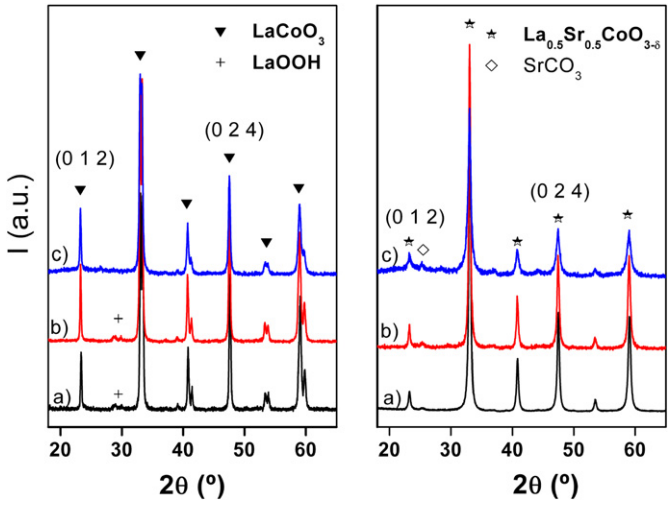

Fig. 2. (Color online). XRD patterns of the $LaCoO_3$ (left) and $La_{0.5}Sr_{0.5}CoO_{3-\delta}$ perovskites (right) under different experimental conditions: (a) original samples after calcinations at 700 °C; (b) perovskites plus carbon after grinding at room temperature; and (c) perovskites after the TPO experiments. (0 1 2) and (0 2 4) parallel planes have been used for the size crystal and $\Delta 2\theta$ calculations.

Table 1
Sizes of crystalline domains calculated from the XRD diffractograms

Sample	FWMH (degrees)[d]	$\Delta 2\theta$ (degrees)[e]	$d_{S(024)}$ (nm)[f]
$LaCoO_3$[a]	0.2433	24.2491	70
$LaCoO_3$ + C[b]	0.2364	24.2639	75
$LaCoO_3$ − PostOx[c]	0.2998	24.2642	60
$La_{0.5}Sr_{0.5}CoO_{3-\delta}$[a]	0.4214	24.2071	29
$La_{0.5}Sr_{0.5}CoO_{3-\delta}$ + C[b]	0.3975	24.1904	31
$La_{0.5}Sr_{0.5}CoO_{3-\delta}$ − PostOx[c]	0.6098	24.1388	18

[a] Original perovskite.
[b] Perovskite after grinding with 10 wt% carbon.
[c] Perovskite after thermal oxidation of carbon at 700 °C in He/O_2 (5%).
[d] Full width at half the maximum height (FWHM) corresponding to the (024) diffraction peak used in the Scherrer calculation of crystalline domain sizes.
[e] Difference in the maximum of the position of peak (012)–peak (024).
[f] Crystalline domain sizes determined from Scherrer equation applied to the (024) diffraction peak. 10% estimated error.

peak and its relative position respect to the (012) one (designated $\Delta 2\theta$) for the samples after they were subjected to different experiments. The sizes calculated from these XRD peaks were also corroborated by SEM images of the samples, both indicating the presence of larger and better-conformed crystalline domains in the nonsubstituted cobaltites and a partial loss of the crystalline structure of the samples after the thermal oxidation treatments (Figs. 1 and 2). The decrease in $\Delta 2\theta$ values shown in Table 1, especially after the TPO reaction, can be directly correlated with an increase of "d" (interplanar distance in Bragg's equation) and indicates an expansion of the crystal lattice [46,47,49].

3.2. TPO of perovskites + carbon mixtures

Fig. 3 shows the TPO profile of carbon and mixtures of the two perovskites plus carbon measured with both the TCD and the calibrated mass spectrometer. (The Y-scale is equivalent for all of the TPO profiles shown in Fig. 3). In this latter case, CO and CO_2 can be differentiated as reaction products. The spectra show that the maximum oxidation rate of carbon occurred at $T = 650$ °C in the absence of the catalysts (cf. Fig. 3a); however, in the presence of the perovskites, total conversion of carbon occurred at 510 °C for $La_{0.5}Sr_{0.5}CoO_{3-\delta}$ and at 540 °C for $LaCoO_3$ (cf. Figs. 3b and 3c). It is also worth mentioning that whereas equivalent amounts of CO and CO_2 were obtained during the direct oxidation of carbon

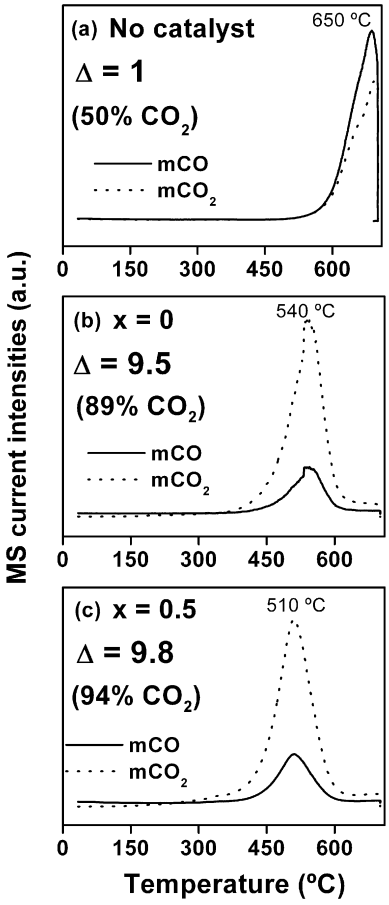

Fig. 3. Evolution of the CO ($m/z = 28$) and CO_2 ($m/z = 44$) mass products formed during the temperature programmed oxidation of carbon nanoparticulates: (a) in the absence of catalysts; (b) in the presence of the non-substituted $LaCoO_3$ perovskite; (c) in the presence of the $La_{0.5}Sr_{0.5}CoO_{3-\delta}$ perovskite; The delta coefficient (Δ) expresses the ratio of areas (CO_2/CO). All the experiments have carried out in tight-contact conditions. The temperature of total oxidation of carbon and the selectivity percentages toward CO_2 are also included.

(~50% CO_2 selectivity), a major conversion to CO_2 occurred (up to 94% CO_2 selectivity in the substituted cobaltite) when the carbon was mixed with the perovskites (cf. Fig. 3). This result is in agreement with findings of previous studies using plasmas plus catalysts in which oxidation of methane progressed to CO_2 in the presence of the $La_{0.5}Sr_{0.5}CoO_{3-\delta}$ catalyst [21]. In addition, TPD experiments [40] helped confirm that the concentration of CO/CO_2 released from the perovskites alone was negligible compared with that from the outlets in the thermal oxidation of carbon.

3.3. EELS analysis of the carbon–perovskite interaction

To gain deeper insight into the phenomena occurring in the perovskite during its interaction with carbon, perovskite–carbon mixtures were analyzed by EELS. Fig. 4 shows the EEL spectra at the cobalt $L_{2,3}$ edge for the two perovskites studied here (Fig. 4a), their mixtures with carbon at room temperature (Fig. 4b), and also after the TPO experiments with He/O_2 (5%) (Fig. 4c). Spectra of the reference compounds used to evaluate the Co^{3+}/Co^{2+} ratio in the samples are also included for comparison. These spectra clearly indicate that the position of the edges shifted from CoO to CoOOH, compounds in which cobalt is in divalent and trivalent oxidation states, respectively [30]. Meanwhile, the edge position of the perovskite samples lies in an intermediate position between the reference compounds, indicating that the average formal oxidation state of cobalt has a intermediate value close to that of

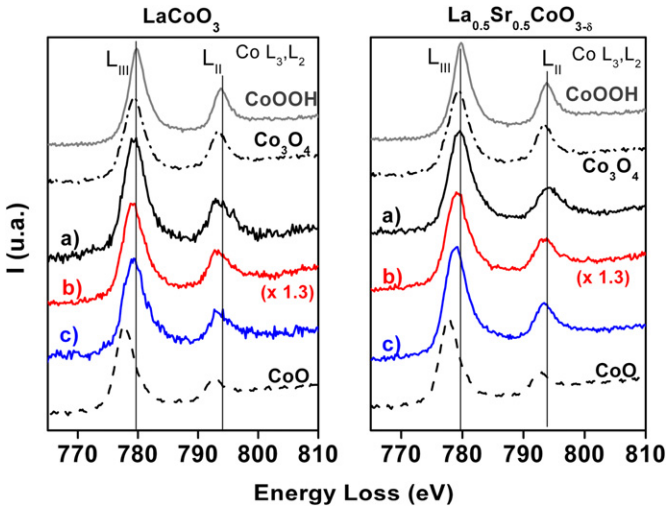

Fig. 4. (Color online). EEL spectra at the cobalt $L_{2,3}$ edge for the non-substituted perovskite (left) and the strontium-substituted perovskite (right) under different experimental conditions: (a) perovskite calcined at 700 °C; (b) perovskite + 10 wt% carbon ground at room temperature; (c) perovskite after the TPO experiments in He/O_2 at 700 °C. The spectra corresponding to the cobalt references are also included. The energy scale of all spectra has been corrected with respect to the lanthanum $M_{4,5}$ edge.

the Co_3O_4 spinel used as a reference. The average oxidation state of cobalt in the perovskites can be estimated more accurately by calculating the intensity ratio between the L_3 and L_2 edges. This method has been used previously to determine the oxidation state of this element in other perovskites and d^6–d^8 mixed-valence compounds [50–53].

Fig. 5a plots of this ratio against the oxidation state of cobalt for a series of reference compounds. The values reported include those determined for the reference compounds used here, along with other values obtained from the literature [52]. Of note, all of the points lay on a single curve, supporting the use of this plot as an empirical reference curve for determining the average oxidation state of cobalt in the perovskite samples. The results of such analysis are plotted in Fig. 5b as the value of this ratio for the two perovskites after they were subjected to different treatments. The values are an average of a series of measurements carried out in different zones of the samples; the error bars account for the dispersion of values found in each case. The evolution of the points indicates that the L_3/L_2 intensity ratio of the perovskites increased from the original material to its physical mixture with carbon at room temperature and, to a greater extent, when this mixture was heated with He/O_2 up to 700 °C. Fig. 5b also shows that this ratio was always smaller for the nonsubstituted $LaCoO_3$ than for the substituted $La_{0.5}Sr_{0.5}CoO_{3-\delta}$. In the former case, the value was close to that expected for a Co^{3+} oxidation state, whereas in the strontium-substituted perovskite, the average oxidation state of cobalt varied between +2.5 and +2.7. This change can be attributed to an increased number of defects (i.e., oxygen vacancies in the structure) generated from the substitution of La^{3+} by Sr^{2+}. The increase in this ratio for the physical mixture, both after grinding and after heating at 700 °C in He/O_2, supports the existence of a reduction process leading to the migration of oxygen from the lattice and, consequently, to a decrease in the average oxidation state of the cobalt (see Fig. 5b).

3.4. XPS analysis of the carbon–perovskite interaction

Because most of the redox processes involving perovskites must start at the surface, it is important to use a surface-sensitive technique, such as XPS, to gain insight into these surface phenomena.

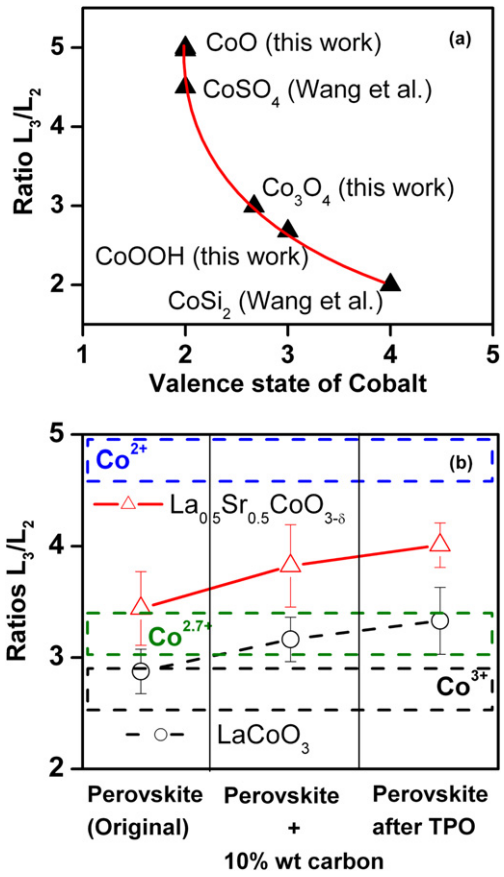

Fig. 5. (Color online). (a) Plots of the intensity ratio of L_3/L_2 for a series of reference compounds (see text); (b) plot of the intensity ratio L_3/L_2 determined for the $LaCoO_3$ and the $La_{0.5}Sr_{0.5}CoO_{3-\delta}$ perovskites after being subjected to different treatments.

We carried out an experiment with the original $La_{0.5}Sr_{0.5}CoO_{3-\delta}$ sample and for this same catalyst after grinding with carbon at room temperature. We chose this perovskite not only because it has greater activity toward carbon oxidation (Fig. 3), but also because similar trends would be expected for the photoemission regions evaluated in the nonsubstituted cobaltite (equivalent composition except for strontium). In both cases, we present in situ results for the original samples, after heating at 400 °C in vacuum and under 0.5 Torr O_2. This latter treatment, although not completely equivalent to the TPO reactions in which the samples were heated up to 700 °C, was anticipated to provide some information about the surface changes occurring in the perovskites at the temperature of the onset of carbon oxidation (cf. Fig. 3b).

Fig. 6 shows the the C 1s, Sr 3d, and La $3d_{5/2}$ photoemission spectra recorded for the perovskite and the perovskite–carbon mixture subjected to the treatments specified. Fig. 7 shows Co $2p_{3/2}$ spectra recorded in the same experiments, along with an analysis of the Co^{3+}/Co^{2+} ratio. Based on the areas of the different spectra and the corresponding sensitivity factors, we can estimate the surface compositions of the samples after the different treatments. Table 2 reports atomic percentages of the monitored elements and some atomic ratios among these elements. The values reveal a deviation in the surface composition of the sample with respect to that of its bulk. Thus, it is particularly interesting that this table shows that the original sample exhibited an increased surface concentration of strontium (i.e., La/Sr ratio of 0.6, quite different from the ratio La/Sr = 1 expected from the bulk composition of the perovskite). This enrichment reverted after the in situ treatments at 400 °C. Another interesting result is that in all cases, the La/Co ratio was higher than that expected from the bulk composition

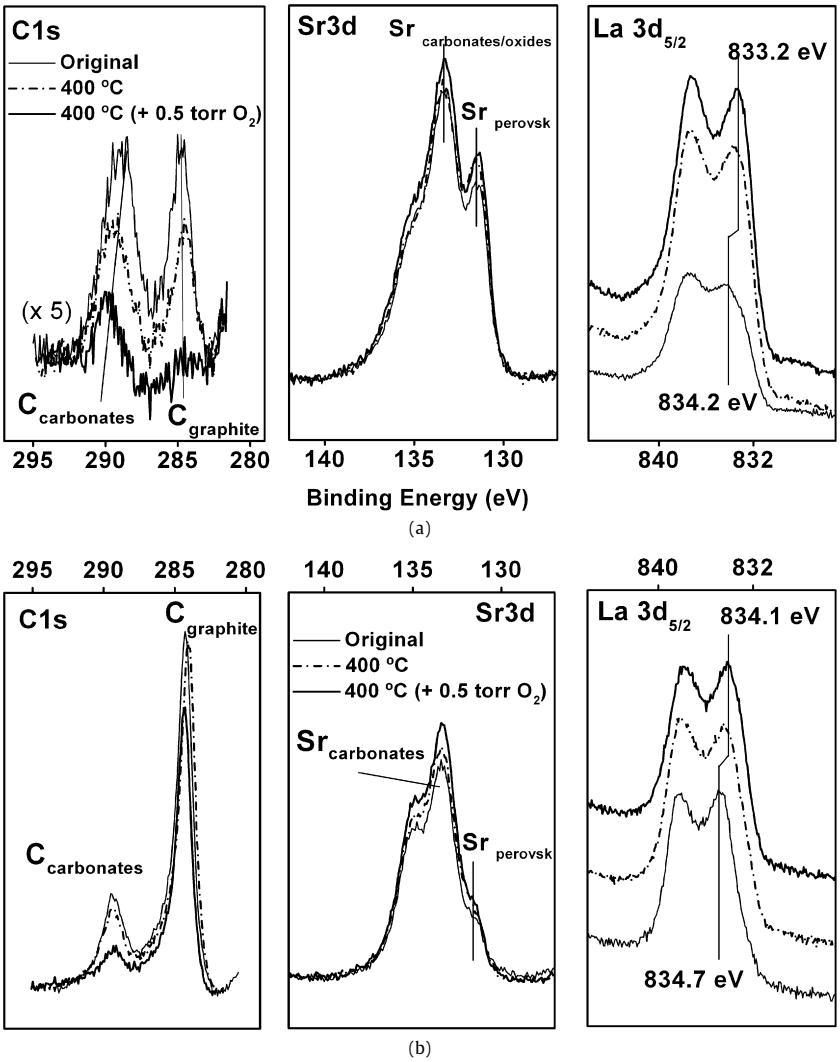

Fig. 6. C 1s, Sr 3d, and La $3d_{5/2}$ photoemission spectra of the $La_{0.5}Sr_{0.5}CoO_{3-\delta}$ perovskite after different (in situ) treatments: (a) original sample before grinding with carbon; (b) perovskite after grinding with 10 wt% carbon at room temperature. The reported spectra correspond to the samples without thermal treatment and after heating at 400 °C in vacuum and in the presence of 0.5 Torr O_2.

Table 2
Surface composition (atomic percentages and atomic ratios) for the $La_{0.5}Sr_{0.5}CoO_{3-\delta}$ perovskite after different treatments as determined by XPS

Sample	Treatments	%C	%O	%Co	La/Co	La/Sr	O/C	%Sr_c[a]	%CO_3^{2-}[b]	O_P/O_{LC}[c]
$La_{0.5}Sr_{0.5}$	25 °C	16.9	56.4	8.3	0.8	0.6	3.3	5.0	12.1	2.1
	400 °C	10.7	50.0	14.9	0.9	1.2	4.7	3.8	6.0	2.7
	400 °C + O_2	2.5	56.5	14.9	1.0	1.1	37.4	6.6	2.5	1.3
$La_{0.5}Sr_{0.5}$ + carbon	25 °C	50.6	32.2	5.7	1.1	1.7	0.6	2.4	13.2	0.9
	400 °C	47.8	30.7	6.7	1.4	1.5	0.7	3.1	12.9	1.3
	400 °C + O_2	38.1	38.4	6.2	1.6	1.3	1.0	4.2	8.4	1.9

[a] Percentage of strontium associated to carbonates.
[b] Total percentage of carbon associated to carbonate species.
[c] Ratio between O species from bulk perovskite lattice (O_P) and low coordination – low density O species (O_{LC}).

(i.e., La/Co = 0.5). It is also noteworthy that grinding the perovskite and the carbon together increased the La at the surface. Here the concentration of this element was less affected by the subsequent thermal treatments compared with the pure sample, as indicated by the shifts in binding energy values shown in Fig. 6.

Along with the percentages and ratios accounting for the surface composition of the samples, Table 2 also reports specific data referring to the C 1s and O 1s spectra resulting from a more accurate analysis of the signals of these elements. From Fig. 6, it is apparent that the Sr 3d and La $3d_{5/2}$ signals were rather complex and must have been formed by the contribution of more than one species. Because under our experimental conditions, these two elements can be present only in the form of Sr^{2+} and La^{3+}, the two species contributing to the spectra must be associated with these ions pertaining to an oxide and a hydroxicarbonate phase [32,54]. The Sr 3d signal clearly points to the existence of two different species of clearly differing binding energies (131.5 and 133.6 eV for the Sr $3d_{5/2}$ peaks). According to the literature, these species can be attributed to Sr^{2+} ions in the perovskite oxide phase and in a hydroxicarbonate phase [32,33,54]. The relative contributions of these two species can be determined by fitting analysis [54]. The results of this evaluation are included in Table 2, which indicates

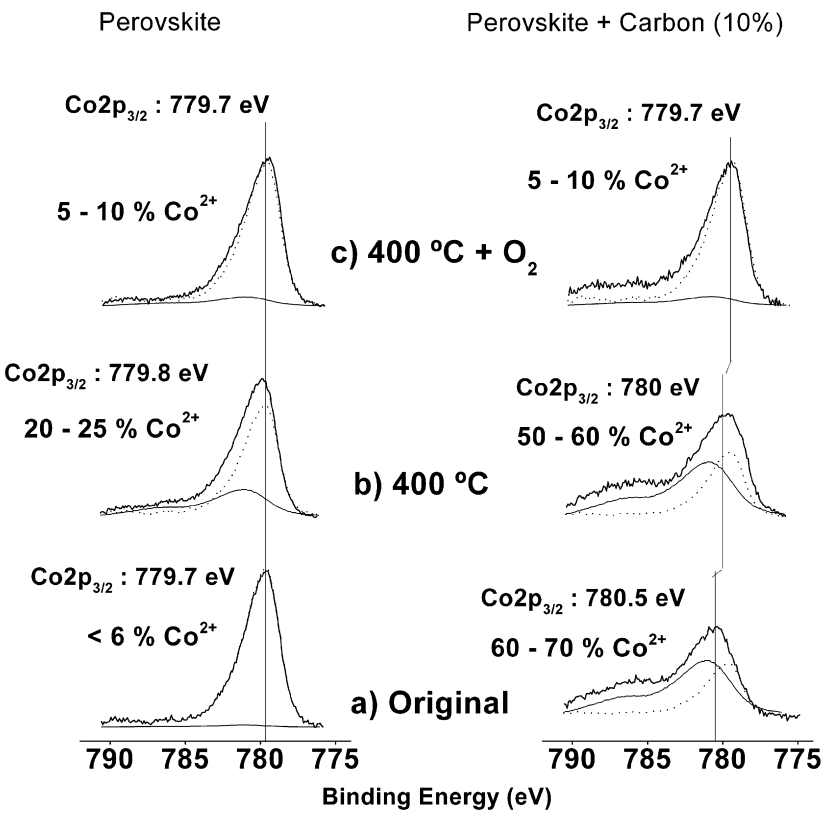

Fig. 7. Co $2p_{3/2}$ photoemission spectra of the $La_{0.5}Sr_{0.5}CoO_{3-\delta}$ perovskite before (left column) and after grinding with 10 wt% carbon (right column) and after different treatments: (a) spectra of the original samples; (b) after heating at 400 °C in vacuum; (c) after heating at 400 °C in the presence of 0.5 Torr O_2. The estimation of the percentage of Co^{3+}/Co^{2+} has been done by linear subtraction of the experimental spectra of the Co^{2+} signal of a reference compound of CoO (see text).

the percentage of strontium atoms (referred to the overall surface composition) associated with the hydroxicarbonate phase.

It is important to mention that after heating at 400 °C, most, if not all, of the hydroxide groups must be removed from the surface, and thus the strontium must be associated with $CO_3^=$ groups at a 1:1 ratio. For simplicity, we assume that this also holds for the original sample before annealing. According to the values given in Table 2 and the shape of the spectra shown in Fig. 6, it is apparent that more strontium was linked to carbonate in the physical mixture with carbon (Fig. 6b, center) than in the original perovskite (Fig. 6a, centre). Table 2 also reports the amount of carbon present on the surface in the form of carbonate species, characterized by a binding energy of 289–290 eV (associated with strontium or lanthanum, or just adsorbed contamination onto the surface). According to these values, the amount of carbonate decreased after the heat treatments, as also demonstrated by the intensity of the C 1s peak at around 290 eV for the samples subjected to heat treatments shown in Fig. 6.

The Co 2p spectra provide interesting information about the chemical state of this element. Fig. 7 shows that cobalt underwent a significant redox transformation when mixed with carbon and also when the sample was heated to increasing temperatures. According to previous reports [54,55], the Co 2p spectrum of the original sample is characteristic of Co^{3+} species (a binding energy of 779.7 eV and the absence of an intense satellite peak at around 786 eV). Heating this sample in vacuum at 400 °C led to a chemical reduction of these species, as evidenced by the fitting analysis of the corresponding spectrum shown in Fig. 7b. The Co^{3+} species were restored when the perovskite was heated in O_2 at this temperature (cf. Fig. 7c).

A completely different situation occurred for the perovskite–carbon mixture (Fig. 7, right). In this case, the spectrum of the mixture before heating showed a considerable reduction of the Co^{3+} species to Co^{2+}, amounting to ca. 60–70% of the total cobalt. This situation was maintained after the mixture was heated in vacuum to 400 °C but was almost completely reversed after it was heated in oxygen at the same temperature. That treatment almost restored the Co 2p spectrum of the original perovskite (cf. Fig. 7a, left and Fig. 7c, right). The most interesting of these results is the fact that Co^{3+} could be reduced to Co^{2+} simply by grinding the perovskite at room temperature with carbon during preparation of the physical mixture (cf. Fig. 7a, right). This result, together with the enhanced carbonation of the surface produced by this treatment (cf. Fig. 6 and Table 2), demonstrate that perovskites exhibit high reactivity toward carbon even at low temperatures. To the best of our knowledge, no analogous results on this solid-solid interaction have been presented to date, despite the fact that other authors have evaluated physical mixtures of catalysts and carbon particles [10,41,42,56,57] or have used milling techniques for fabricating perovskites [58–60]. Also of note, a similar grinding experiment in the absence of catalyst did not show any change in the spectra thus discarding mechanical effects associated to the grinding process.

XPS analysis of the O 1s spectra provided additional information about the evolution with temperature of the surface of perovskites when mixed with carbon. Fig. 8 shows a series of fitted O 1s spectra corresponding to the samples subjected to the same treatments as those reported in Figs. 6 and 7. Fitting was carried out under the assumption of four different species of oxygen in the experimental spectra. For the analysis, the position and width of the corresponding bands were kept fixed throughout the series of spectra. According to the literature, the first band at 528.3 eV (hereafter called O_P) can be associated with oxide species of the perovskite lattice [54,55], the band at 529.5 eV can be ascribed to oxide ions of segregated single oxides of the cations present in the sample [33,54,61], and the band at 531 eV can be attributed to

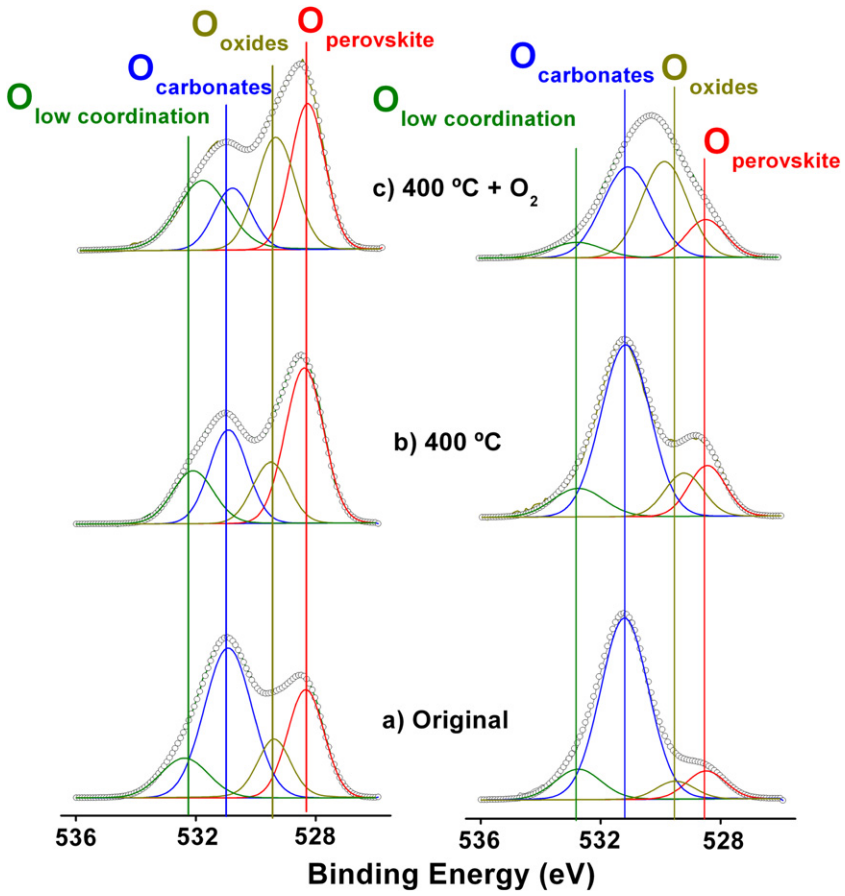

Fig. 8. (Color online). Fitted O 1s photoelectron spectra of the $La_{0.5}Sr_{0.5}CoO_{3-\delta}$ perovskite before (left column) and after grinding with 10 wt% carbon (right column) and after different treatments: (a) spectra of the original samples; (b) after heating at 400 °C in vacuum; (c) after heating at 400 °C in the presence of 0.5 Torr O_2.

oxygen in the form of hydroxide or carbonate species [54,55,62–64]. The intensity of this latter band was not left free during the analysis, but rather was assumed to be fixed as a function of the amount of carbonate species present in the sample, as reported in Table 2. Thus, the intensity of this band was estimated according to $I_{O\text{-}C} = I_C 3(\sigma_O/\sigma_C)$, where I_C is the intensity of the C 1s peak due to carbonates [62] and σ_O and σ_C are the sensitivity factors of oxygen and carbon, respectively.

Following this fitting procedure, it is apparent that some intensity of the O 1s peak remained, which can be justified only by the presence of another band at a higher binding energy (i.e., 532.4 eV). The results of previous analyses of O 1s spectra of cobalt spinels and defective cerium oxide [36,37,65] allow us to tentatively attribute this extra band to oxide ions with low electron density, likely because they are in a very low coordination state and/or are associated with cation vacancies in the oxide structure [36,37,65]. The fitted O 1s spectra of the pure perovskite samples after the different treatments show that, in agreement with the data given in Table 2 and the C 1s spectra shown in Fig. 6, heating at 400 °C produced significant decarbonation of the surface along with a simultaneous increase in the concentration of oxide species in the perovskite and the segregated oxides. Because the percentage of strontium associated with carbonate species remained practically unmodified after the treatments (cf. Fig. 8 and Table 2), the formation of surface patches of lanthanum oxide seems to be the main result of surface decarbonation. Simultaneously, the spectrum in Fig. 8 (left) demonstrate an increase in the intensity of the band associated with low-electron density oxide ions.

In the perovskite–carbon mixture, the initial O 1s spectrum was dominated by oxide pertaining to carbonate species, in agreement with the data for the other elements (Fig. 8 and Table 2). Heating this sample in vacuum produced only a slight decrease in the intensity of the carbonate species. Oxides linked to carbonate species were diminished significantly only after heating in oxygen to 400 °C, accompanied by an increased intensity of the peak due to oxide ions from segregated oxides. The decrease in the O_P/O_{LC} ratio with respect to the original samples (cf. Table 2) can be seen as another indication of the partial destruction of the perovskite lattice due to its interaction with carbon during preparation of the physical mixture.

4. Discussion

The TPO experiments on carbon alone or the perovskite–carbon mixture demonstrate that in the presence of this catalyst, the oxidation temperature decreased by ca. 140 °C (i.e., from 650 to 510 °C; see Fig. 3). Moreover, the observed increase in the selectivity toward CO_2 indicates that the perovskites had moderate efficiency as oxidation catalysts of soot particles [4]. Other catalysts, including cobalt-containing oxides [12,13,24], spinel-like structures [8,25], and perovskites with Cr and Li [3], have demonstrated better catalytic behavior by reducing the temperature of carbon combustion to below 400 °C, some of them even under loose contact conditions. Previous studies have linked the oxidation capacity of the perovskites with the ionic mobility of $O^{=}$ species that migrate to the surface as an effect of temperature [4,19]. This hypothesis has been proved with experiments using isotopically marked oxygen in the gas phase that demonstrated the evolution of products with two kinds of oxygen [23]. It seems that the ionic migration of oxide ions occurs through the formation of oxygen vacancies occupied by other oxide ions of the lattice to compensate for the defect of charge [4,19,35,66],

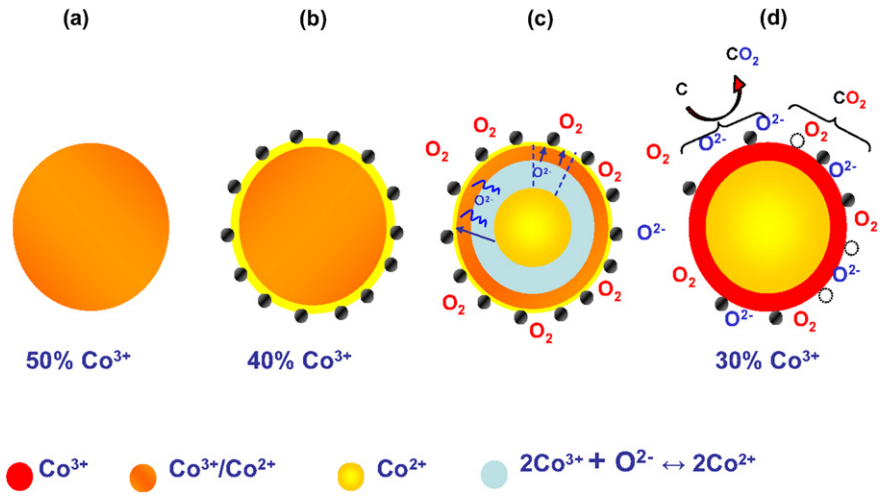

Fig. 9. (Color online). Scheme of the cobalt oxidation states distribution within the perovskite as a consequence of the interaction and reaction with carbon particulates: (a) perovskite as prepared (without carbon); (b) after grinding at room temperature; (c) intermediate state during the heating treatment at 400 °C in the presence of 0.5 Torr O_2; (d) final state of the perovskite after the complete removal of carbon by prolonged thermal oxidation. The expressed percentages of cobalt are deduced from the EELS calculations described in Section 3.3.

$$(Co^{3+} - O^{=} - Co^{3+}) \rightarrow \left(Co^{2+} - [V_O] - Co^{2+}\right), \quad (1)$$

where V_O represents an anionic vacancy.

Our EELS and XPS experiments have shown that the different treatments produce changes in the chemical state of cobalt and in the distribution of the elements at the surface. These changes can be accounted for by the model shown schematically in Fig. 9. We elaborated on this model by taking into account the different proving depths of the EELS and XPS techniques. EELS can be considered bulk-sensitive, whereas XPS is sensitive only to the outermost sample layers. The ratio L_3/L_2 determined from the EEL spectra allow us to determine the average valence state of the cobalt and, in an indirect way, calculate the amount of anionic vacancies in the structure, particularly for the substituted perovskite (cf. Fig. 5b).

Based on the EELS calculations (cf. Fig. 5), we estimate that in the original strontium-substituted perovskite, half of the cobalt was in a trivalent state, and the other half should correspond to divalent states. Therefore, we must assume that to maintain electroneutrality, the structure contains a significant concentration of anionic vacancies. Previous studies combining TEM and EELS found that in defective perovskites with a Brownmillerite-like structure, an ordered distribution of oxygen atoms and anionic vacancies along the lattice is possible [50,67]. In other cases, the distribution is not ordered, and oxygen defects and cobalt ions with different oxidation states are randomly distributed in the perovskite structure [52]. In our samples, XRD revealed that the perovskite structure was maintained even after the reaction at 700 °C (Fig. 2c). In addition, the finding that the (012) and (024) peaks became closer after these treatments (see Table 1) suggests an expansion of the unit cell. This finding is congruent with the substitution of Co^{3+} ($r = 0.63$ Å) by Co^{2+} ($r = 0.74$ Å) cations [68]. The observed changes were smaller in the nonsubstituted perovskite, in agreement with the larger size of the crystalline domains and also the predominance of the Co^{3+} species in this sample (cf. Fig. 7 and Table 1). Thus, the model shown in Fig. 9a accounts for the original perovskite where there is a homogeneous distribution of Co^{2+} and Co^{3+} species.

Fig. 9b accounts for the solid–solid reaction occurring during the preparation of the perovskites–carbon mixture. The partial reduction of cobalt detected by XPS reveals considerable surface reactivity toward carbon even at room temperature. The maintenance of the perovskite structure after grinding (cf. Fig. 2b). This is demonstrated schematically in the model shown in Fig. 9b by an external layer with a high concentration of Co^{2+} species (ca. 70% according to the XPS analysis; cf. Fig. 7), leading to a 40% concentration of Co^{3+} species as estimated by EELS. Our XPS analysis also suggests the existence of additional phenomena. According to the fitting analysis of the O 1s spectra (cf. Fig. 8, left column), the original sample had a significant contribution of oxygen species from the perovskite lattice (i.e., the band at 528.3 eV) [54,55], along with the presence of low-electron density oxide species appearing at higher binding energies (i.e., the band at 532.5 eV) [36]. The existence of this singular surface oxygen can be associated with low-coordinated oxygen atoms at special sites on the surface with a higher covalence of the Co–O bond, as was proposed previously for other polycrystalline cobalt oxides [36]. Recent TPD experiments also have accounted for the existence of oxygen species not only from the lattice network, but also from dislocations and grain frontiers (i.e., pseudodefective perovskites and/or oxides) [40,58–60]. We believe that this species may favor the reaction of perovskite with carbon particles after grinding at room temperature and somehow may be associated with the typically reported anionic vacancies responsible for the active role of perovskites in oxidation reactions [4,19,58–60].

On the other hand, comparing the XPS results for the original sample and the physical mixture reveals evidence pointing to partial destruction of the perovskite structure at the surface due to the reaction between perovskite and carbon. Table 2 indicates a decrease in the O_P/O_{LC} ratio from 2.1 to 0.9 between the original perovskite and the physical mixtures. This indicates an increased presence of low-coordination species of oxygen at the surface, likely due to the partial destruction of the perovskite structure at the surface (see Fig. 8). Moreover, the change in the Co 2p spectrum shown in Fig. 7, characterized by a shift toward higher binding energies and the appearance of a satellite at ca. 786 eV, clearly indicates a reduction of cobalt. Consequently, the following overall reaction can be proposed to account for the interaction process occurring at the surface during the grinding of the perovskites and the carbon particles (cf. Fig. 9b):

$$(Co^{3+} - O^{=} - Co^{3+}) + C \rightarrow \left(Co^{2+} - [V_O] - Co^{2+}\right) + CO_x. \quad (2)$$

Our data provide additional evidence supporting the partial destruction of the perovskite lattice in the outer layers of the oxide particles in the physical mixture. In fact, the XPS spectra shown in Figs. 6 and 8 and the results given in Table 2 indicate that mixing with carbon enhanced the carbonation state of the perovskite surfaces. This finding can be explained by assuming that

the perovskite structure was partially destroyed during the chemical reduction of the Co^{3+} species, which would favor carbonation of the segregated lanthanum and strontium oxides with the atmospheric CO_2/H_2O [10].

The effect of heating at 400 °C in the presence O_2 is considered in the model schemes of Figs. 9c and 9d. According to the literature [4,19], increasing temperature facilitates the elimination of surface hydroxicarbonates (cf. Fig. 6) and the migration of O^{2-} species from the bulk to the surface. This explains the partial decrease in the overall oxidation state of cobalt for the perovskites after the TPO experiments, as detected by EELS (cf. Fig. 5), as well as the 140 °C decrease in the overall temperature of carbon oxidation in the presence of perovskite (Fig. 3). In the presence of oxygen, the carbon particulates in contact with the catalysts were oxidized by both the O_2 added as a reactant and the contribution of the O^{2-} ions provided by the perovskite lattice. This led to oxygen depletion within the perovskite grains, as well as an additional decrease in the average oxidation state of cobalt as determined by EELS (cf. Figs. 9c and 9d).

The other effect of heating in the presence of O_2 demonstrated by the XPS analysis is the transformation of surface (La, Sr)-carbonates into their oxide counterparts. Both the increment of the O 1s fitted band at 529 eV (cf. Fig. 8) and the binding energy shifts in the La 3d spectrum from La-carbonate to La-oxide species point in that direction [31,54]. Probably some of these oxides were inherently segregated to the surface of the perovskites because of the preparation method used [32]. Nonetheless, the destruction of the perovskite structure by reduction with carbon and its subsequent reoxidation by O_2 allowed the additional formation of both finely dispersed oxides (not detectable by XRD) and pseudodefective perovskites structures containing sites for labile oxygen species associated with the higher binding energy band at 532.4 eV (cf. Fig. 8).

The final state of the cobaltites after the TPO experiments revealed a nonstoichiometric perovskite that maintained its structure but with a higher amount of vacancies within its lattice. EELS calculations of the valence state of cobalt confirmed a reduction in the overall valence state (cf. Fig. 7b). This evidence might seem to contradict the finding that, according to the XPS results, cobalt underwent additional oxidation after being heated with oxygen (cf. Fig. 7). But we believe that, according to the model scheme in Fig. 9d, this simply indicates that the Co^{3+} enrichment was concentrated in the outer parts of the perovskites while its bulk was depleted in oxide ions due to migration to the surface through the anionic vacancies. This spillover mechanism facilitated the creation of "additional oxygen" species that actively participated in the oxidation of carbon, leading to a major selectivity toward CO_2 as a byproduct [4,14,19,21,59,69]. Similar behavior also has been observed in CeO_2-based catalysts [14,48,70].

5. Conclusion

We have shown that the cobaltites prepared by a spray pyrolysis method are suitable catalysts for the oxidation of finely divided carbon particles simulating the effect of soot. TPO experiments under tight contact conditions demonstrated moderate activity of the cobaltites, with a ca. 140 °C reduction in the oxidation temperature of carbon with respect to the results obtained in the absence of catalysts. Perovskites and fine carbon particles may react even at room temperature when they are ground together to form a physical mixture but with only mechanically induced effects discounted, because no surface reduction was detected in the absence of carbon. As a result of this reaction, the perovskite surfaces are partially reduced and strongly carbonated. The combination of XPS and EELS techniques has provided evidence that at higher temperatures, significant migration of O^{2-} lattice species toward the surface occurs, thereby increasing the potential number of active sites for the oxidation of carbon and the selectivity toward CO_2. This migration of oxygen ions is marked by an overall depletion of oxygen ions in the bulk of the grains of perovskites (supported by EELS) and a higher oxidation state of cobalt at the surface (indicated by XPS). In addition, a new oxygen species has been identified at the surface of the cobaltites by XPS. This species is attributed to low-electron density oxide ions likely located in low-coordination sites and is compatible with the existing oxygen species also evidenced by TPD experiments.

Acknowledgments

This work was supported by the Spanish Ministry of Science and Education (projects PPQ2001-3108 and ENE2004-01660 and a doctoral fellowship for J.H.). The authors thank Cabot for providing the carbon nanoparticles used in this study, and Mr. Macías for providing technical assistance with the XPS experiments.

References

[1] G. Corro, J.L.G. Fierro, F. Bañuelos Romero, Catal. Commun. 7 (2006) 867.
[2] S.S. Hong, J.S. Yang, G.D. Lee, React. Kinet. Catal. Lett. 66 (1999) 305.
[3] N. Russo, D. Fino, G. Saracco, V. Specchia, J. Catal. 229 (2005) 459.
[4] D. Fino, N. Russo, G. Saracco, V. Speechia, J. Catal. 217 (2003) 367.
[5] S. Biamino, P. Fino, D. Fino, N. Russo, C. Badini, Appl. Catal. B Environ. 61 (2005) 297.
[6] A. Carrascull, I.D. Lick, E.N. Ponzi, M.I. Ponzi, Catal. Commun. 4 (2003) 124.
[7] A.F. Ahlstrom, C.U.I. Odenbrand, Appl. Catal. 60 (1990) 157.
[8] J. Liu, Z. Zhao, C.M. Xu, H. Wang, React. Kinet. Catal. Lett. 87 (2005) 107.
[9] G. Mul, J.P.A. Neeft, M. Makkee, F. Kapteijn, J.A. Moulijn, in: Catalysis and Automotive Pollution Control Iv, vol. 116, Elsevier, Amsterdam, 1998, p. 645.
[10] J.P.A. Neeft, M. Makkee, J.A. Moulijn, Appl. Catal. B Environ. 8 (1996) 57.
[11] D. Uner, M.K. Demirkol, B. Dernaika, Appl. Catal. B Environ. 61 (2005) 334.
[12] C.A. Querini, M.A. Ulla, F. Requejo, J. Soria, U.A. Sedrán, E.E. Miró, Appl. Catal. B Environ. 15 (1998) 5.
[13] P.G. Harrison, I.K. Ball, W. Daniell, P. Lukinskas, M. Cespedes, E.E. Miro, M.A. Ulla, Chem. Eng. J. 95 (2003) 47.
[14] A. Bueno-López, K. Krishna, M. Makkee, J.A. Moulijn, J. Catal. 230 (2005) 237.
[15] R. Cousin, S. Capelle, E. Abi-Aad, D. Courcot, A. Aboukais, Appl. Catal. B Environ. 70 (2007) 247.
[16] Y. Zhang, Z. Xiaoting, L. Sui, Catal. Commun. 7 (2006) 855.
[17] Y. Zhang, Z. Xiaoting, Catal. Commun. 7 (2006) 523.
[18] D. Fino, N. Russo, C. Badini, G. Saracco, V. Specchia, AIChE J. 49 (2003) 2173.
[19] T. Nakamura, M. Misono, Y. Yoneda, Bull. Chem. Soc. Jpn. 55 (1982) 394.
[20] R.J.H. Voorhoeve, D.W. Johnson, J.P. Remeika, P.K. Gallagher, Science 195 (1977) 827.
[21] J.L. Hueso, J. Cotrino, A. Caballero, J.P. Espinós, A.R. González-Elipe, J. Catal. 247 (2007) 288.
[22] D. Fino, N. Russo, C. Badini, G. Saracco, V. Specchia, Korean J. Chem. Eng. 20 (2003) 451.
[23] L. Borovskikh, G. Mazo, E. Kemnitz, Solid State Sci. 5 (2003) 409.
[24] C.A. Querini, L.M. Cornaglia, M.A. Ulla, E.E. Miro, Appl. Catal. B Environ. 20 (1999) 165.
[25] D. Fino, N. Russo, G. Saracco, V. Specchia, J. Catal. 242 (2006) 38.
[26] E. López-Navarrete, A. Caballero, V.M. Orera, F.J. Lázaro, M. Ocaña, Acta Mater. 51 (2003) 2371.
[27] N. Closset, R. v. Doorn, H. Kruidhof, J. Boeijsma, Powder Diffr. 11 (1996) 31.
[28] R.F. Egerton, Electron Energy-Loss Spectroscopy in the Electron Microscope, vol. 2, Plenum Press, New York, 1996.
[29] C.S. Mcardell, A.T. Stone, J. Tian, Environ. Sci. Technol. 32 (1998) 2923.
[30] R. Pozas, T.C. Rojas, M. Ocaña, C.J. Serna, Clays Clay Miner. 52 (2004) 760.
[31] V. Belliere, G. Joorst, O. Stephan, F.M.F. de Groot, B.M. Weckhuysen, J. Phys. Chem. B 110 (2006) 9984.
[32] G. Munuera, A.R. González-Elipe, J.P. Espinós, E. López-Molina, Surf. Interface Anal. 15 (1990) 693.
[33] V. Young, T. Otagawa, Appl. Surf. Sci. 20 (1985) 228.
[34] J.H. Shirley, Phys. Rev. B 138 (1965) 979.
[35] S. Kaliaguine, V. Szabo, A. Van Neste, J.E. Gallot, M. Bassir, R. Muzychuk, Electrochemical and Chemical Reactivity of Amorphous and Nanocrystalline Materials, vol. 377, 2001, p. 39.
[36] V.M. Jiménez, A. Fernández, J.P. Espinós, A.R. González-Elipe, J. Electron Spectrosc. Relat. Phenom. 71 (1995) 61.
[37] V.M. Jiménez, J.P. Espinós, A.R. González-Elipe, Surf. Interface Anal. 26 (1998) 62.

[38] A. Caballero, J.J. Morales, A.M. Cordón, J.P. Holgado, J.P. Espinós, A.R. González-Elipe, J. Catal. 235 (2005) 295.
[39] J.L. Hueso, A.R. González-Elipe, J. Cotrino, A. Caballero, J. Phys. Chem. A 109 (2005) 4930.
[40] R. Pereñíguez, J.L. Hueso, A. Caballero, J.P. Holgado, F. Gaillard, in preparation.
[41] J.P.A. Neeft, M. Makkee, J.A. Mouljin, Fuel 77 (1998) 111.
[42] J.P.A. Neeft, O.P. vanPruissen, M. Makkee, J.A. Moulijn, Appl. Catal. B Environ. 12 (1997) 21.
[43] I. Atribak, I. Such-Basáñez, A. Bueno-López, A. García García, Catal. Commun. 8 (2007) 478.
[44] P. Scherrer, Nachr. Ges. Wiss. Gott. 26 (1918) 98.
[45] A. Bueno-López, I. Such-Basáñez, C.S.M. de Lecea, J. Catal. 244 (2006) 102.
[46] A.D. Krawitz, Introduction to Diffraction in Materials Science and Engineering, Wiley, New York, 2001.
[47] H. Lipson, H. Steeple, Interpretation of X-Ray Power Diffraction Patterns, Macmillan, New York, 1970.
[48] I. Atribak, A. Bueno-López, A. García-García, Catal. Commun. 9 (2008) 250.
[49] D. Martínez-Martínez, Ph.D. thesis, 2007, p. 38.
[50] R.F. Klie, Y. Ito, S. Stemmer, N.S. Browning, Ultramicroscopy 86 (2001) 289.
[51] Z.L. Wang, J. Bentley, N.D. Evans, Micron 31 (2000) 355.
[52] Z.L. Wang, J.S. Yin, Y.D. Jiang, Micron 31 (2000) 571.
[53] J.L. Hueso, Ph.D. thesis, 2007.
[54] P.A.W. van der Heide, Surf. Interface Anal. 33 (2002) 414.
[55] L.G. Tejuca, J.L.G. Fierro, J.M.D. Tascón, Adv. Catal. 36 (1989) 237.
[56] B.R. Stanmore, J.F. Brilhac, P. Gilot, Carbon 39 (2001) 2247.
[57] P. Ciambelli, P. Corbo, M. Gambino, V. Palma, S. Vaccaro, Catal. Today 27 (1996) 99.
[58] S. Royer, D. Duprez, S. Kaliaguine, Catal. Today 112 (2006) 99.
[59] S. Royer, D. Duprez, S. Kaliaguine, J. Catal. 234 (2005) 364.
[60] V. Szabo, M. Bassir, J.E. Gallot, A.V. Van Neste, S. Kaliaguine, Abstr. Pap. Am. Chem. Soc. 221 (2001) U474.
[61] R.P. Vasquez, J. Electron Spectrosc. Relat. Phenom. 56 (1991) 217.
[62] A.R. González-Elipe, J.P. Espinós, A. Fernández, G. Munuera, Appl. Surf. Sci. 45 (1990) 103.
[63] M. Machkova, N. Brashkova, P. Ivanov, J.B. Carda, V. Kozhukharov, Appl. Surf. Sci. 119 (1997) 127.
[64] K. Tabata, I. Matsumoto, S. Kohiki, J. Mater. Sci. 22 (1987) 1882.
[65] J.P. Holgado, G. Munuera, J.P. Espinós, A.R. González-Elipe, Appl. Surf. Sci. 158 (2000) 164.
[66] V. Szabo, M. Bassir, A. Van Neste, S. Kaliaguine, Appl. Catal. B Environ. 43 (2003) 81.
[67] M. James, D. Cassidy, D.J. Goossens, R.L. Withers, J. Solid State Chem. 177 (2004) 1886.
[68] R.D. Shannon, C.T. Prewitt, Acta Cryst. B Struct. 26 (1970) 1046.
[69] T. Nakamura, M. Misono, Y. Yoneda, Chem. Lett. (1981) 1589.
[70] I. Atribak, I. Such-Basáñez, A. Bueno-López, A. García-García, J. Catal. 250 (2007) 75.